Roll-to-roll fabrication of hierarchical superhydrophobic surfaces

Sunilkumar Khandavalli, Patrick Rogers, and Jonathan P. Rothstein

Citation: Appl. Phys. Lett. **113**, 041601 (2018); doi: 10.1063/1.5037946
View online: https://doi.org/10.1063/1.5037946
View Table of Contents: http://aip.scitation.org/toc/apl/113/4
Published by the American Institute of Physics

Roll-to-roll fabrication of hierarchical superhydrophobic surfaces

Sunilkumar Khandavalli, Patrick Rogers, and Jonathan P. Rothstein[a)]
Department of Mechanical and Industrial Engineering, University of Massachusetts, Amherst, Massachusetts 01003, USA

(Received 29 April 2018; accepted 7 July 2018; published online 23 July 2018)

In this letter, we report a roll-to-roll fabrication method to develop a hierarchical nanopatterned superhydrophobic surface. The hierarchical pattern includes a primary micropattern with an overlayed secondary nanopattern. The primary pattern of 15–30 μm length scales was fabricated through UV nanoimprint lithography. The secondary nanopattern of 20 nm size was generated through a subsequent scalable spray coating with hydrophobic silica nanoparticles to create a nanoscale random roughness over the primary pattern. The secondary nanocoating over the primary pattern resulted in an enhanced contact angle resulting in superhydrophobicity and reduced hysteresis. Freezing droplet measurements performed have demonstrated a fivefold increase in the time for the droplet to freeze on a superhydrophobic surface compared to a primary hydrophobic structure. *Published by AIP Publishing.* https://doi.org/10.1063/1.5037946

The hierarchical micro- and nano-architectured surfaces are of great scientific and technological interest due to interesting surface physics, hydrodynamics,[1–5] and many engineering applications.[3,6] A hierarchical structure is composed of two or more layers of different size scales, random or well defined structure. Many examples in nature present hierarchical micro- and nanostructures, often more complex, which include lotus leaf,[1] water striders,[7] beetles,[8] and butterfly wings.[9] Superhydrophobic surfaces are one of the classes of hierarchical structures that have attracted immense interest due to many potential applications, such as self-cleaning,[1] anti-icing,[10] drag reduction,[2,11,12] corrosion resistance,[13] and anti-fouling.[3] Superhydrophobic surfaces have a large water contact angle $>150^\circ$ and low contact angle hysteresis, $\theta_A - \theta_R < 10^\circ$, where θ_A is an advancing contact angle and θ_R is a receding contact angle. Superhydrophobicity is the result of a combination of micro- or nanoscale roughness and a natively hydrophobic surface. The large contact angle between the water and the hydrophobic surface prevents water droplets from wetting into the features, but instead they remain suspended over the micro- or nano-scaled air pockets of the pattern. The air trapped in between the pattern features reduces the net solid-water interfacial contact area, simultaneously increasing the advancing contact angle and reducing the contact angle hysteresis. The design of a superhydrophobic structure with a hierarchical nature, compared to a single structure, has been found to have superior properties, such as an increased advancing contact angle, lower contact angle hysteresis,[1] improved drag reduction,[14] and greater stability and robustness.[15–17]

Numerous fabrication approaches have been utilized in order to create hierarchical superhydrophobic surfaces[6] both chemical and physical methods, which include e-beam lithography,[18] molding and imprinting,[19] chemical[20] and reactive-ion etching,[15] self-assembly,[21] deposition,[22] ultrasonically assisted synthesis,[23] photo-lithography,[24] and growth of nanowires.[25] A scalable fabrication process of potentially low cost and fast manufacturing is very important in order to fully realize the potential of superhydrophobic surfaces, particularly for large-area applications. However, a large fraction of fabrication approaches in the literature involve steps that are slow and/or difficult to scale for large-area manufacturing.[14,18,26–28] There have been some reports on roll-to-roll or scalable approaches to fabricate single-layer/structure superhydrophobic surfaces.[19,29–34] However, very limited reports exist on the fabrication of multilayer superhydrophobic architectures through roll-to-roll processes either single step patterning[3] or multi-step fabrication approaches. Li *et al.*[3] have demonstrated the fabrication of a hierarchical superhydrophobic pattern consisting of nanopillars (several hundreds of nanometers in size) on a wrinkle pattern (tens of microns in order) through a single UV nanoimprinting step. Such single-step approaches to create a hierarchical structure might be fast and economical; however, each patterning approach has a certain allowable resolution. Using a combination of patterning approaches via the multi-step process allows a more flexible design of hierarchical architectures and a wider range of pattern feature length scales. In this letter, we demonstrate a continuous roll-to-roll approach to fabricate a hierarchical superhydrophobic surface with secondary nanostructures, up to $\sim$10 nm in size, over a primary micropattern, tens of microns in order, with enhanced self-cleaning and anti-icing properties.

A schematic of the roll-to-roll fabrication process to create a hierarchical superhydrophobic surface is shown in Fig. 1. First, a primary microstructure was created by patterning through roll-to-roll UV nanoimprint lithography (R2R UV-NIL). The R2R UV-NIL experimental tool used was a custom designed setup (Carpe Diem Technologies, MA, USA), the same as that adopted by Li *et al.*[3] For the UV NIL process, a UV resist solution was formulated based on thiol-ene chemistry. The formulation is the same as that prepared by Li *et al.*[3] It contains monomers of pentaerythritol tetrakis(3-mercaptopropionate) (PETMP, purchased from Sigma-Aldrich) and 1,3,5-triallyl-1,3,5-triazine-2,4,6(1H,3H,5H)-trione (TTT, purchased from Sigma-Aldrich) mixed at an equimolar ratio in 30 wt. %

a)rothstein@ecs.umass.edu

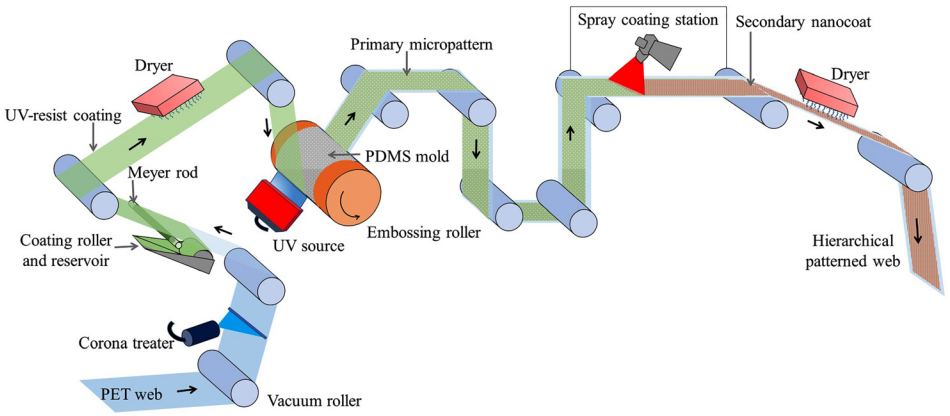

FIG. 1. Schematic of the roll-to-roll fabrication process adopted to fabricate the hierarchical patterned surface.

propylene glycol monomethyl ether acetate solvent (PGMEA, purchased from Sigma-Aldrich). Other additives in the mixture include 1 wt. % benzoin methyl ether (BME, purchased from Sigma-Aldrich) as a photoinitiator and 1 wt. % 1H,1H,2H,2H-Perfluorodecyl acrylate (PFDA, purchased from Alfa Aesar) to create a low surface energy component.

In order to create a primary pattern through the UV-NIL process, the formulated UV resist solution was first coated onto a corona treated polyethylene terepthalate (PET) web using a Mayer rod coater (rod no. 20) to obtain a wet coating thickness of 25 μm at a web speed of 25 cm/min. The UV resist coated web was then passed through a drying unit to remove the PGMEA solvent. Next, a desired micropattern was imprinted onto the UV resist coat through an embossing step. Two micropatterns were used in this study. One is a ridge pattern with a spacing of 15 μm, a height of 25 μm, and an aspect ratio of 0.6. Another is a circular post pattern with a diameter of 30 μm, a center-to-center distance of 60 μm, a height of 25 μm, and an aspect ratio of 1.2. For the imprinting process, polydimethoxysiloxane (PDMS) molds with the ridges and the posts micropattern were first fabricated from the respective 152.4 mm (6′) silicon master molds developed through the conventional photolithography process. The PDMS adhesive was mixed with the crosslinker at a ratio of 1:10 and degassed to remove air bubbles. The mixture was cast into the silicon master mold, cured in an oven at 60 °C for 12 h, and then was peeled-off from the master mold. This process was repeated to obtain multiple PDMS replica. In order to create a single 48 cm continuous mold for the R2R UV-NIL process, the obtained multiple PDMS replicas were cast and cured as a single mold using PDMS. The resulting R2R PDMS mold was then cured onto a PET film using PDMS as an adhesive.

The fabricated PDMS roll mold was wound onto the embossing roller using a double sided tape. The micropattern was imprinted onto the UV coated web continuously and subsequently cured using a UV lamp (Omnicure 2000, EXFO). The cured pattern was then peeled-off from the embosser to obtain a primary micropattern. Examples of the patterned surfaces that were transferred from the PDMS mold to UV resist on the PET film are shown in Fig. 2. The micropatterns were imaged using scanning electron microscopy (JEOL JSM-7001F). In Fig. 2(a), the 15 μm wide microridge with a spacing of 15 μm is shown. In Fig. 2(b), the circular posts having a diameter of 30 μm and a center-to-center spacing of 60 μm on a square lattice are shown. Both patterns had a height of 25 μm and aspect ratios of 0.6 and 1.2, respectively.

The advancing and receding contact angle measurements were performed on the roll-to-roll fabricated surfaces using a sessile drop method and are presented in Fig. 3. The advancing contact angle of water on the PET film was $\theta_A = 75°$. Adding the hydrophobic UV resist coating without texture

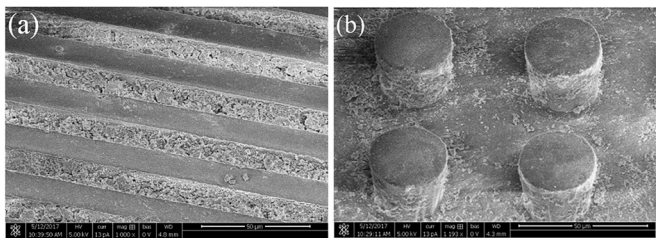

FIG. 2. SEM images of different micropatterns with silica nanoparticle surface coating, which include (a) ridges of 15 μm width and 25 μm height and (b) circular posts of 30 μm diameter, 60 μm center-to-center distance, and 25 μm height.

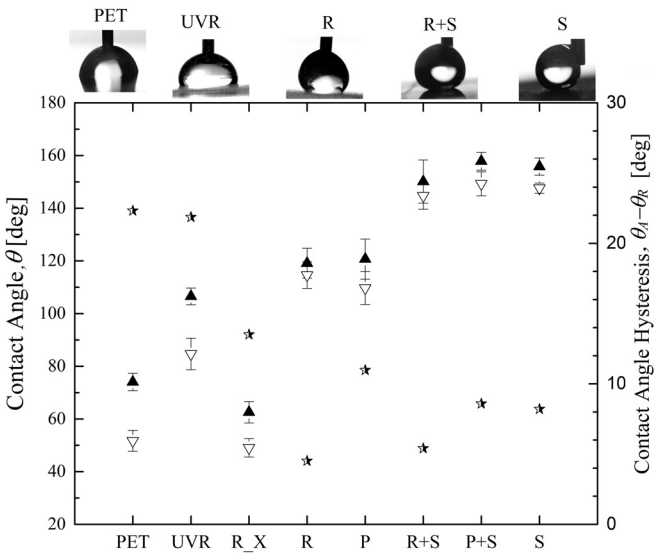

FIG. 3. Advancing contact angle, θ_A (▲), receding contact angle, θ_R (▽), and contact angle hysteresis, $\theta_A - \theta_R$ (★), measurements on different surfaces. The measurements include the smooth PET film, UV resin (UVR), cross-microridge direction (R_X), in-microridge direction (R), microposts (P), nanoparticle coating over PET (S), nanoparticle coating over ridges (R + S), and nanoparticle coating over posts (P + S).

increased the advancing contact angle up to $\theta_A = 113°$. With the imprinted micropatterns, the advancing contact angle was found to further increase by more than 10% compared to a planar UV-resist coated PET film. For example, the surface populated with micropost had an advancing contact angle of 120°, while the advancing contact angle of the microridges measured in the direction parallel to the microridges was found to be 119°. This increase is due to the introduction of an air-water interface along the contact line between the droplet and the micropatterned surface.[18] The micropatterned surfaces also show a significant reduction in contact angle hysteresis, from over $\theta_H > 20°$ for the smooth hydrophobic UV-resist surface to $\theta = 10°$ or less for the micropatterned surfaces. We also note that the advancing contact angle of the ridge pattern was found to be very sensitive to the direction it was measured, whether parallel or perpendicular to the ridge direction. The advancing contact angle measured in the cross-ridge direction was found to be nearly half the value of the measurement parallel to the ridge direction, $\theta_A = 63°$. This can be expected as the contact line encounters very different boundary conditions in the directions parallel and perpendicular to the microridge direction.[35] In the cross-ridge direction, the contact-line can pin along the top-corner of the ridge, while along the ridge direction, the contact line can smoothly advance. The discontinuity of the contact line across the surface patterned with microposts tends to reduce the effect of pinning and orientation effects.

Next, a secondary nanostructure was overlayed onto the primary imprinted microstructure through a spray coating process in order to create a hierarchical superhydrophobic surface topography. The material used to create the secondary nanostructured coating was a perfluorinated silica nanoparticle solution. The solution was synthesized through co-hydrolysis of tetraethylorthosilicate (TEOS, Sigma-Aldrich) and a fluorinated alkyl silane (FAS) (Dynasylan F8261, graciously supplied by Evonik, NJ, USA).[36] The FAS and TEOS were mixed at a mass ratio of 1:10, in a solution with 10% ethanol and 20% D.I water. An aqueous solution of 1 mM NAOH was added as a catalyst and the solution was sonicated for 30 min and then mechanically stirred for an additional 6 h. As the reaction proceeded, perfluorinated silica nanoparticles precipitated from the solution.

The synthesized particle dispersion was directly used to spray coat onto the moving web, after the UV-nanoimprinting step. The web was then passed through the drying station to remove the solvent. This process resulted in a secondary structure with nanoroughness due to aggregated fluorinated-silica nanoparticles overlayed onto the primary micropattern, as shown in the SEM images in Fig. 2. The morphology of the secondary nanostructure was characterized through AFM (Bruker Multimode). The AFM height image and a line profile are shown in Fig. 4. The average roughness and rms roughness were estimated using WSXM software[37] and were ~7.5 nm and 9.5 nm, respectively.

The advancing and receding contact angle measurements of the resulting hierarchical superhydrophobic surfaces containing the secondary nanocoating superimposed on top of the primary imprinted microposts and microridges are presented in Fig. 3. With the introduction of the additional

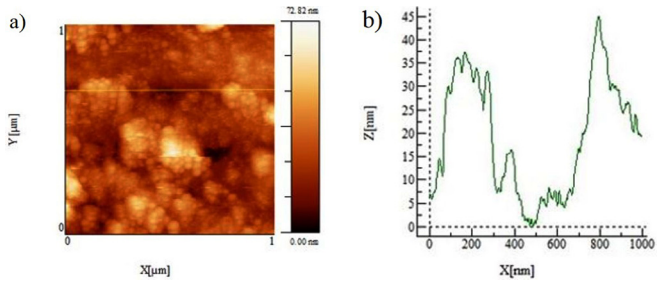

FIG. 4. AFM (a) height image and (b) line profile of silica nanoparticle coating onto a primary microridge pattern.

surface topography from secondary nanocoating, the advancing contact angles were found to significantly increase by more than 25% resulting in what would be classically defined as a superhydrophobic surface with an advancing contact angle $\theta_A > 160°$ and a contact angle hysteresis of less than $\theta_H < 10°$. This enhancement in the advancing contact angle and the resulting superhydrophobicity is due to the presence of the nanoroughness morphology associated with the aggregated hydrophobic silica nanoparticles. This is consistent with observations in the literature regarding hierarchical surfaces with both micron and nanometer length scale surface topography.[1,18,36]

Interestingly, the addition of the secondary nanoroughness was found to eliminate the orientation dependence of the contact angle measurements on the microridge patterned surfaces. The advancing contact angle and the hysteresis were found to be nearly identical in the direction both parallel and perpendicular to the microridge direction. This suggests that the contact line dynamics are dominated by the nanoroughness for these hierarchical surfaces. More evidence for that can be seen in the contact angle measurements of pure nanocoating on PET without a primary micropattern, which is also presented in Fig. 3. The pure nanocoating alone presented was found to be superhydrophobic with an advancing contact angle and low contact angle hysteresis. The question then might be asked, why is the micron-sized pattern needed at all. There are a number of advantages to hierarchical superhydrophobic surfaces compared to superhydrophobic surfaces with just nanoroughness. For the surfaces tested here, the wear resistance or adhesion of the pure nanoparticle coating both on the PET substrate and on the UV-resin coated PET substrate was observed to be very poor, whereas, the surfaces with nanocoating overlayed onto the primary micropattern were found to be quite stable and resistant to light abrasion. Such improved wear resistance of hierarchical superhydrophobic surfaces consisting of a secondary nanostructure on a primary micropatterned structure was reported in the literature.[16,17] Additionally, in many applications where a drag reduction is important, micron length surface patterns are critical for optimizing the performance of superhydrophobic surfaces.[2]

Droplet freezing experiments were also studied on these surfaces. Several water droplets of 10 μl were slowly placed onto the different substrates in a freezer at a temperature of -10 ± 0.2 °C. The droplets were visually observed with time using a high speed video camera to determine the freezing time. The measurements were taken for at least ten droplets

in order to perform a proper statistical analysis. The droplet freezing times on the different surfaces are presented in Fig. 5. On the smooth PET film, the droplets were found to freeze after $t_f = 1.5$ min. The freezing time measured for the smooth UV-resist coated surface and the patterned surfaces, both microridge and micropost, was all similar and within the uncertainty of the measurements at about $t_f = 9$ min. This is a significant increase in more than a factor of four, compared to the PET surface. This could be a result of the increased contact angle and the subsequent reduction in the contact area between the drop and the substrate. For the hierarchical superhydrophobic surfaces with the secondary nanocoating, the droplet freezing time was delayed even further, by a factor of two or three, compared to the smooth UV-resist coated surface or the micro-patterned surfaces. The hierarchical micropost surface required $t_f = 16$ min to freeze, while the hierarchical microridge surface required $t_f = 27$ min. Interestingly, the surface coated with only nanoparticles and no additional microstructure was found to have the longest freezing time of $t_f = 43$ min. This delay in the droplet freezing time with the increasing contact angle with a substrate is consistent with the literature.[38] However, the dependence of the freezing time with the details of the hierarchical superhydrophobic surface topography is not so easily explained. The increase in the freezing time for superhydrophobic surface cases has been argued in the literature to be a result of the reduced heat transfer due to the presence of an insulating trapped air layer beneath the drop.[39] Others have argued that the delay in freezing is the result of a reduction in the nucleation sites for the onset of freezing.[40] More recently, some have argued that the increased freezing time is a result of the decrease in the droplet-solid interfacial contact area and the increased contact angle, which dramatically reduces the heat transfer rate into the drop.[41,42]

In conclusion, we have demonstrated a continuous roll-to-roll fabrication approach to develop a hierarchical superhydrophobic surface, containing a secondary nanopattern overlayed over a primary micropattern. The introduction of the secondary nano-pattern was shown to result in superhydrophobicity with a low contact angle hysteresis and a dramatic increase in the freezing time of a water droplet placed on the substrate. Although the secondary nanocoating alone exhibited self-cleaning and anti-icing properties, the presence of the primary pattern could improve the wear resistance of the secondary nanostructure.[16,17] Further, a dual structure offers more tunability to design functional surfaces for a variety of applications.[14,43] The roll-to-roll fabrication approach presented here can be used for large-area manufacturing of a variety of hierarchical micro- and nano- structured surfaces with water-repellent, anti-icing, and drag reducing properties. Additionally, it provides a flexible platform for developing a host of functional hierarchical structures for applications of interest.

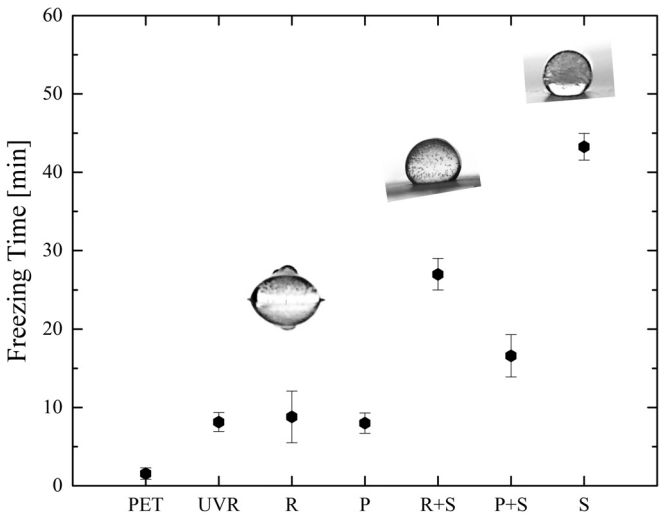

FIG. 5. Freezing time of the water droplet on different surfaces. The measurements include the smooth PET film, UV resin (UVR), microridges (R), microposts (P), nanoparticle coating over PET (S), nanoparticle coating over ridges (R + S), and nanoparticle coating over posts (P + S).

The authors would like to thank National Science of Foundation for funding the current project through the Center for Hierarchical Manufacturing at UMASS under Grant No. CMMI-1025020 and Louis Raboin and Dr. Alexander Ribbe for assisting with SEM and AFM measurements.

[1]B. Bhushan, Y. C. Jung, and K. Koch, Langmuir **25**, 3240 (2009).
[2]J. P. Rothstein, Annu. Rev. Fluid Mech. **42**, 89 (2010).
[3]Y. Li, J. John, K. W. Kolewe, J. D. Schiffman, and K. R. Carter, ACS Appl. Mater. Interfaces **7**, 23439 (2015).
[4]Y. Liu, L. Moevius, X. Xu, T. Qian, J. Yeomans, and Z. Wang, Nat. Phys. **10**, 515–519 (2014).
[5]M. P. Murphy, S. Kim, and M. Sitti, ACS Appl. Mater. Interfaces **1**, 849 (2009).
[6]X.-M. Li, D. Reinhoudt, and M. Crego-Calama, Chem. Soc. Rev. **36**, 1350 (2007).
[7]D. L. Hu, B. Chan, and J. Bush, Nature **424**, 663 (2003).
[8]T. Nørgaard and M. Dacke, Front. Zool. **7**, 23 (2010).
[9]Y. Zheng, X. Gao, and L. Jiang, Soft Matter **3**, 178 (2007).
[10]L. Cao, A. K. Jones, V. K. Sikka, J. Wu, and D. Gao, Langmuir **25**, 12444 (2009).
[11]D. Song, R. J. Daniello, and J. P. Rothstein, Exp. Fluids **55**, 1783 (2014).
[12]J.-H. Kim, H. P. Kavehpour, and J. P. Rothstein, Phys. Fluids **27**, 032107 (2015).
[13]T. Rezayi and M. H. Entezari, J. Colloid Interface Sci. **463**, 37 (2016).
[14]E. Taghvaei, A. Moosavi, A. Nouri-Borujerdi, M. Daeian, and S. Vafaeinejad, Energy **125**, 1 (2017).
[15]Y. Kwon, N. Patankar, J. Choi, and J. Lee, Langmuir **25**, 6129 (2009).
[16]Y. C. Jung and B. Bhushan, ACS Nano **3**, 4155 (2009).
[17]Y. Xiu, Y. Liu, D. W. Hess, and C. P. Wong, Nanotechnology **21**, 155705 (2010).
[18]J. Feng, M. T. Tuominen, and J. P. Rothstein, Adv. Funct. Mater. **21**, 3715 (2011).
[19]J. Li, Z. Jing, F. Zha, Y. Yang, Q. Wang, and Z. Lei, ACS Appl. Mater. Interfaces **6**, 8868 (2014).
[20]Y. Xiu, L. Zhu, D. W. Hess, and C. P. Wong, Nano Lett. **7**, 3388 (2007).
[21]K. Koch, B. Bhushan, Y. C. Jung, and W. Barthlott, Soft Matter **5**, 1386 (2009).
[22]Y. Xiu, L. Zhu, D. W. Hess, and C. P. Wong, Langmuir **22**, 9676 (2006).
[23]H. Chen, E. Kern, C. Ziegler, and A. Eychmüller, J. Phys. Chem. C **113**, 19258 (2009).
[24]C. Greiner, E. Arzt, and A. del Campo, Adv. Mater. **21**, 479 (2009).
[25]H. Ko, Z. Zhang, K. Takei, and A. Javey, Nanotechnology **21**, 295305 (2010).
[26]Q.-X. Zhang, Y.-X. Chen, Z. Guo, H.-L. Liu, D.-P. Wang, and X.-J. Huang, ACS Appl. Mater. Interfaces **5**, 10633 (2013).
[27]M. Gong, Z. Yang, X. Xu, D. Jasion, S. Mou, H. Zhang, Y. Long, and S. Ren, J. Mater. Chem. A **2**, 6180 (2014).
[28]L. Passoni, G. Bonvini, A. Luzio, A. Facibeni, C. E. Bottani, and F. Di Fonzo, Langmuir **30**, 13581 (2014).
[29]M. Leitgeb, D. Nees, S. Ruttloff, U. Palfinger, J. Götz, R. Liska, M. R. Belegratis, and B. Stadlober, ACS Nano **10**, 4926 (2016).

[30]A. Telecka, S. Murthy, L. Schneider, H. Pranov, and R. Taboryski, ACS Macro Lett. **5**, 1034 (2016).
[31]N. V. Motlagh, F. Birjandi, J. Sargolzaei, and N. Shahtahmassebi, Appl. Surf. Sci. **283**, 636 (2013).
[32]B. J. Sparks, E. F. T. Hoff, L. Xiong, J. T. Goetz, and D. L. Patton, ACS Appl. Mater. Interfaces **5**, 1811 (2013).
[33]S. Wang, Y. Yang, Y. Zhang, X. Fei, C. Zhou, Y. Zhang, Y. Li, Q. Yang, and Y. Song, J. Appl. Polym. Sci. **131**, 39735 (2014).
[34]S. H. Lee, J. H. Lee, C. W. Park, C. Y. Lee, K. Kim, D. Tahk, and M. K. Kwak, Int. J. Precis. Eng. Manuf. **1**, 119 (2014).
[35]H. Kusumaatmaja, R. J. Vrancken, C. W. M. Bastiaansen, and J. M. Yeomans, Langmuir **24**, 7299 (2008).
[36]H. Wang, J. Fang, T. Cheng, J. Ding, L. Qu, L. Dai, X. Wang, and T. Lin, Chem. Commun. **0**, 877 (2008).
[37]I. Horcas, R. Fernández, J. M. Gómez-Rodríguez, J. Colchero, J. Gómez-Herrero, and A. M. Baro, Rev. Sci. Instrum. **78**, 013705 (2007).
[38]L. Huang, Z. Liu, Y. Liu, Y. Gou, and L. Wang, Exp. Therm. Fluid Sci. **40**, 74 (2012).
[39]P. Tourkine, M. Le Merrer, and D. Quéré, Langmuir **25**, 7214 (2009).
[40]A. Alizadeh, M. Yamada, R. Li, W. Shang, S. Otta, S. Zhong, L. Ge, A. Dhinojwala, K. R. Conway, V. Bahadur, A. J. Vinciquerra, B. Stephens, and M. L. Blohm, Langmuir **28**, 3180 (2012).
[41]F. Alizadeh-Birjandi, E. Tavakoli-Dastjerdi, J. S. Leger, S. H. Davis, J. P. Rothstein, and H. P. Kavehpour, "Ice formation delay on penguin feathers," Langmuir (to be published).
[42]Z. Liu, X. Zhang, H. Wang, S. Meng, and S. Cheng, Exp. Therm. Fluid Sci. **31**, 789 (2007).
[43]Y. Zhang, Y. Chen, L. Shi, J. Li, and Z. Guo, J. Mater. Chem. **22**, 799 (2012).